ARTICLES

Phase diagrams of bcc alloys at low temperatures with ballistic atom movements

L. B. Hong and B. Fultz
Division of Engineering and Applied Science, 138-78, California Institute of Technology, Pasadena, California 91125
(Received 3 January 1995; revised manuscript received 29 March 1995)

Kinetic Monte Carlo simulations were used to determine the steady states of equiatomic bcc alloys with first- and second-nearest-neighbor (1NN and 2NN) effective pair interactions. Atom movements occurred with a vacancy mechanism, and were of two types: thermal and ballistic. The phase diagram in the space spanned by the 1NN and 2NN interaction strengths was determined for thermal atom movements alone, and with some ballistic atom movements. With increasing temperature, the region of $B32$ phase receded against the adjacent regions of $B2$ order and unmixed states. With some ballistic atom movements, however, the region of $B32$ order encroached on the adjacent regions of $B2$ order and unmixed state. The shifts in phase boundaries are attributed to differences in how the internal energies of the different phases are affected by ballistic atom movements. Local fluctuations in the internal energy density in the presence of ballistic atom movements caused two-phase regions in the phase diagram.

I. INTRODUCTION

Lattice models have been used to obtain phase diagrams for many years.[1] Although a rigorous result for the phase diagram of an ordering alloy at finite temperatures exists only for a square lattice with first-nearest-neighbor (1NN) effective pair interactions,[2] exact results for the thermodynamic ground state (i.e., at $T=0$) are available for alloys with 1NN and 2NN pair interactions.[3,4] These ground-state diagrams, which present regions of stable phase in a space spanned by the 1NN and 2NN interaction strengths, are expected to change with temperature. In the present paper we calculate the change in the phase boundaries at low temperatures for the bcc alloy with 1NN and 2NN pair interactions. These changes are small.

The main goal of the present study was to identify shifts in phase boundaries in the presence of "ballistic atom movements." Our approach was to use Monte Carlo simulations to attain the steady states at long times. With conventional activated state rate theories for the atom movements, where an atom movement depends on a Boltzmann probability characteristic of its local chemical environment, these steady states of the alloy will be states of thermodynamic equilibrium. Martin and co-workers have proposed a model that extends activated state rate theory by adding random ballistic atom movements to the conventional thermal ones.[5–12] In the presence of ballistic atom movements, the alloy does attain a steady state (as expected for a Markovian system[13]), but this state is not the state of thermodynamic equilibrium. In essence, Martin's model includes two classes of atom movements: thermal movements that occur at fixed finite temperature, and ballistic movements that occur at an infinite temperature. This is an oversimplification for most physical systems, but the model does allow for phenomena that are not predicted by thermal atom movements at a fixed temperature. Previous work has identified shifts in phase boundaries,[5–12,14,15] such as suppression of the critical temperature for order-disorder phase transitions,[5–7,15] changes in the order of the transition,[6–10] and other nonequilibrium microstructural features in the steady states of alloys with ballistic atom movements.[11,12,14] The problem of alloy steady states in the presence of ballistic atom movements has been suggested as a basis for understanding physical phenomena such as the steady states of an alloy undergoing ion irradiation at elevated temperatures,[16] or high-energy ball milling.[17] Phase transitions in the presence of ballistic atom movements are examples of "kinetic phase transitions" that are of wide interest in physical or biological systems.[18]

In the present work we studied the effects of ballistic atom movements on three states of an equiatomic bcc alloy with 1NN and 2NN effective pair potentials: $B2$ order, $B32$ order, and an unmixed bcc alloy (denoted "umx") with different regions having high concentrations of each of the two atom species. We used Monte Carlo simulations with a controlled fraction of ballistic atom movements to find changes in the phase boundaries in the space spanned by the strengths of the 1NN and 2NN pair interactions. We found that ballistic atom movements cause much larger shifts in phase boundaries than does temperature alone. More surprisingly, the directions of change for the $B32$ phase boundaries caused by ballistic atom movements were opposite in sign from the changes caused by temperature alone. This shows that an alloy subjected to ballistic atom movements cannot be considered merely to have a higher effective temperature. We also found that ballistic atom movements sometimes

0163-1829/95/52(9)/6230(8)/$06.00

cause sharp phase boundaries to open into two-phase regions.

II. MONTE CARLO SIMULATIONS

Our Monte Carlo simulations were performed on bcc lattices, typically of $32\times32\times32\times2=65\,536$ sites, which were occupied with a nearly equal number of A and B atoms and one vacancy. Both 1NN and 2NN pairwise interactions between atoms were considered. In our notation, V_{MNi} ($M,N=A$ or B and $i=1$ or 2) was the iNN M-N pair potential in units of k_BT, and the iNN pairwise exchange potential V_i was defined as

$$V_i \equiv V_{AAi}+V_{BBi}-2V_{ABi} , \tag{1}$$

and the ratio of pair potentials, v, was defined as

$$v \equiv V_2/V_1 . \tag{2}$$

For a bcc alloy with 1NN and 2NN effective pair interactions, three thermodynamic states of the alloy are expected in thermodynamic equilibrium at low temperatures, depending on the ratio v.[3,4] These three states are the $B2$ ordered phase, the $B32$ ordered phase, and an unmixed alloy with two bcc regions of nearly all A or all B atoms. At $T=0$, the phase boundaries between the three regions are at $v=\{-\frac{2}{3},+\frac{2}{3},\infty\}$, and most of our work was with alloys near these three phase boundaries $\{\text{umx}/B32, B32/B2, B2/\text{umx}\}$. Unless stated otherwise, these three regions of v were obtained with pair potentials having approximate values: $\{(V_{AA1}=-1, V_{BB1}=-1, V_{AA2}=+1.32, V_{BB2}=0), (V_{AA1}=+1, V_{BB1}=+1, V_{AA2}=+1.32, V_{BB2}=0), (V_{AA1}=-0.06, V_{BB1}=0, V_{AA2}=-1, V_{BB2}=-1)\}$. For all simulations, $V_{AB1}=0$ and $V_{AB2}=0$.

The vacancy served as the agent for both thermal and ballistic atom movements. Our mechanism was described in detail previously,[14,15] but is reviewed briefly here. Each Monte Carlo step was a competition between all z ($z=8$ for bcc lattices) 1NN atoms of the vacancy to exchange sites with the vacancy. First, a random number was used to determine if the upcoming jump was a ballistic jump, according to the preset fraction of the ballistic jumps, f. If the jump was determined to be ballistic, one of the z 1NN atoms was selected randomly to exchange sites with the vacancy. Otherwise, each of the z 1NN atoms had its own thermal jump probability, p_j ($0\le p_j\le 1$), determined by the thermal jump frequencies, $\{\omega_j\}$, of all z 1NN atoms:

$$p_j=\omega_j/\sum_{j'=1}^{z}\omega_{j'} . \tag{3}$$

Another random number, weighted by the probability p_j, was then used to select one of the z 1NN atoms to perform the thermal jump.

The thermal jump frequencies, $\{\omega_j\}$, were calculated according to activated state rate theory:

$$\omega_j \propto \exp[-(E^*-E_j)/k_BT] \propto \exp(E_j/k_BT) , \tag{4}$$

with E^* the saddle-point energy for the jump, and E_j the total pairwise interaction energy of the jth 1NN atom in its initial state:

$$E_j=N_{AA1}V_{AA1}+N_{BB1}V_{BB1}+N_{AB1}V_{AB1} +N_{AA2}V_{AA2}+N_{BB2}V_{BB2}+N_{AB2}V_{AB2} , \tag{5}$$

where N_{MNi} was defined as the number of iNN M-N pairs involving the jth atom.

To characterize the structural evolution during the transitions, long-range order (LRO) parameters for $B32$ order, $B2$ order, and the unmixed state were calculated with a simulated x-ray-diffraction procedure described previously.[14] Nonzero intensities of the superlattice peaks $(\frac{1}{2}\frac{1}{2}\frac{1}{2})$ and (100) measured the extent of $B32$ and $B2$ order, respectively, while the excess intensity of the transmitted beam (000) [minus the (000) intensity of the random alloy] measured the degree of unmixing. We defined LRO parameters, L_{B32}, L_{B2}, and L_{umx}, as the square root of the intensities of the $(\frac{1}{2}\frac{1}{2}\frac{1}{2})$, (100), and (000) peaks, respectively, after normalizing by the intensity of the fundamental (110) peak of the random alloy. For our choices of scattering factor and normalization, the three order parameters, L_{B32}, L_{B2}, and L_{umx} ranged from 0 to 1, with 1 corresponding to perfect $B32$ or $B2$ order, or complete unmixing, respectively.

III. RESULTS

Figure 1 presents the evolution of the order parameters L_{B32} and L_{umx} in an alloy whose state of thermodynamic equilibrium was an unmixed state. The evolution of the order parameters for the thermodynamic case with $T>0$ and $f=0$ are shown by the thick curves. Kinetics allows the transient formation of $B32$ order, and for a brief time this transient $B32$ order is stronger than the state of unmixing. This is not surprising, since unmixing requires long-range diffusion, which is less expedient than the formation of $B32$ order.[19–21] Nevertheless, the state of the alloy after long times was the unmixed state, as expected in thermodynamic equilibrium. (As seen in Fig. 1 for $f=0$, towards the end of our simulations the order parameter for the unmixed state, L_{umx}, was still evolving.

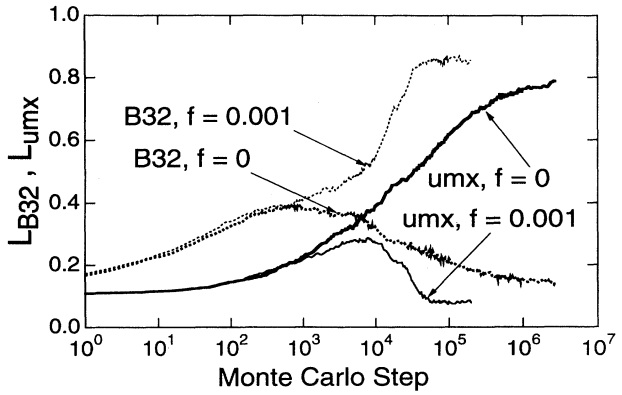

FIG. 1. Time evolution of L_{umx} (solid) and L_{B32} (dashed) for $v=-0.66$ with $f=0$ and 0.001.

The long times and large lattice sizes required to attain two large regions were difficulties in the present work, and some of our estimates of the steady-state values of L_{umx} may be slightly low.)

Figure 1 also presents the evolution of order parameters in an alloy with the same effective pair potentials, but with a small fraction of ballistic jumps ($f=0.001$). The early stages of ordering, which have large relaxations of internal energy, are unaffected by the presence of a small fraction of ballistic jumps. After about 10^4 Monte Carlo steps, however, the small fraction of ballistic jumps causes the two order parameters to be reversed in magnitude from their values for the thermodynamic case of $f=0$. The ballistic jumps cause $B32$ order to be favored over the unmixed state.

A set of Monte Carlo runs with different values of f were performed for $\nu=-0.66$ as in Fig. 1. The steady-state values attained by the order parameters L_{B32} and L_{umx} in these alloys are presented as a function of f in Fig. 2. The figure shows that at about $f=0.0003$, there is a crossover of the state of order where the ballistic jumps cause a change in the final state from an unmixed alloy to a $B32$ ordered alloy. Figure 2(b) presents the steady-state internal energy density of the same alloys as a function of f. The internal energy density undergoes a distinct drop at $f=0.0003$. This drop indicates that in the presence of ballistic jumps, the internal energy of the unmixed state is larger than that of the state $B32$ order. Examination of the alloys showed that this was due in part to antisite defects, but the importance of an internal interface between A and B atoms in the unmixed alloy is discussed in Sec. IV A.

Results analogous to those for Fig. 2 are presented in Fig. 3 for L_{B32} and L_{B2} near the $B32/B2$ phase boundary (near $\nu=+\frac{2}{3}$). Some results for $B32$-$B2$ equilibrium were

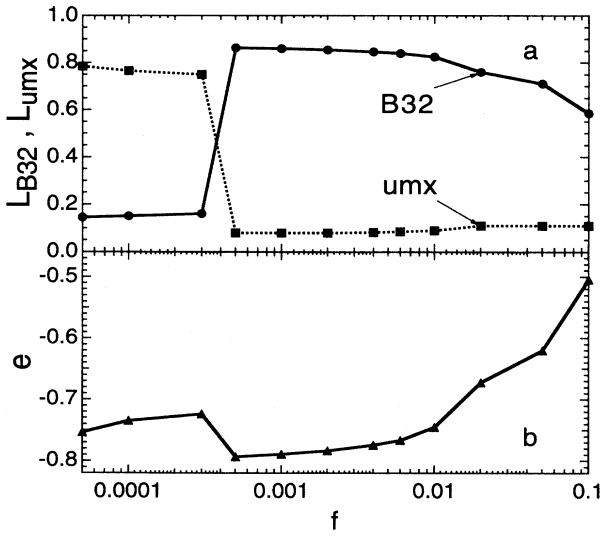

FIG. 2. (a) The steady-state values of L_{umx} (squares) and L_{B32} (circles) during kinetic evolution with $\nu=-0.66$ as functions of f. (b) The corresponding steady-state internal energy per atom, e, as a function of f.

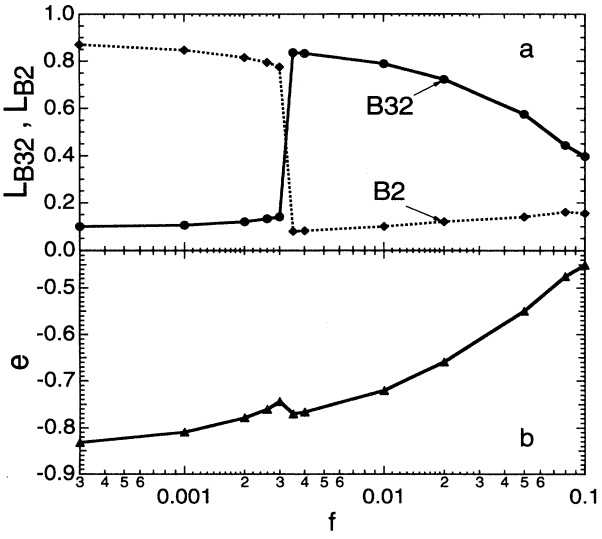

FIG. 3. (a) The steady-state values of L_{B2} (diamonds) and L_{B32} (circles) during kinetic evolution with $\nu=+0.66$ as functions of f. (b) The corresponding steady-state internal energy per atom, e, as a function of f.

presented previously,[14] such as the crossover in Fig. 3(a) from a steady state of $B2$ order to a steady state of $B32$ order at $f=0.003$. Figure 3(b) presents an additional result of the internal energy density, e, of the alloy versus f, showing that a drop in the internal energy density also occurs at $f=0.003$. Near the transition, the internal energy density is higher for the $B2$ state of order than for the $B32$ state of order. In Sec. IV B, we argue that this change in internal energy density is caused by differences in the defect densities of the two phases.

Figure 4 presents a compilation of all our results on the steady-state values of the order parameters L_{B32} and L_{umx} for alloys of $f=\{0,0.01,0.02,0.05,0.10\}$ for various ν near the $B32$/umx phase boundary. For the ther-

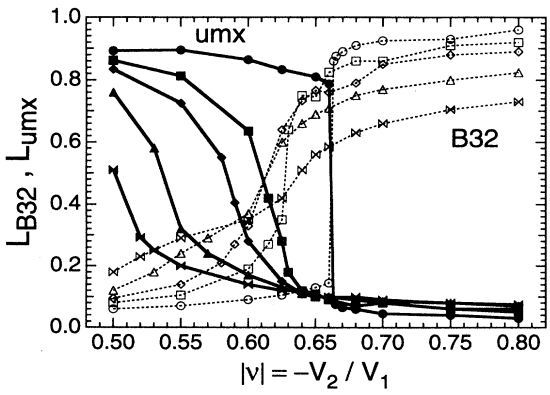

FIG. 4. The steady-state values of L_{umx} (solid) and L_{B2} (dashed) during kinetic evolution with $f=\{0,0.01,0.02,0.05,0.1\}$ with markers {circles, squares, diamonds, triangles, and bow ties} as functions of ν.

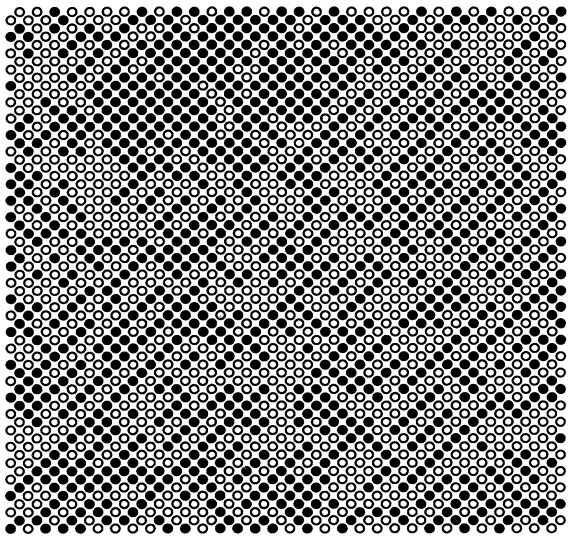

FIG. 5. Projection of two adjacent (200) planes of an alloy in steady state with $\nu=-0.6285$ and $f=0.01$, showing two-phase coexistence. Corner and center atoms of standard cubic bcc unit cell are projected. A and B atoms are shown as black or white circles. Unmixed regions are found in the upper left as regions of black or white, whereas banded regions indicate $B32$ order. Order parameters of the alloy were $L_{B32}=0.58$ and $L_{\text{umx}}=0.23$.

modynamic case of $f=0$, we find that the phase boundary is sharp, and occurs at $\nu=-0.6633$. We define ν_c as the crossover point of the two curves L_{B32} and L_{umx}. Notice that with increasing f, ν_c shifts to lower values of $|\nu|$, primarily because of the strong shift of L_{umx} with f.

Examination of selected planes of the alloy showed another important effect of ballistic atom movements on the state of order. The steady states of thermodynamic alloys ($f=0$) were a state of pure $B32$ order or a pure unmixed state. For $f>0$, however, the steady states of the alloy were heterogeneous, showing regions of $B32$ order in contact with unmixed regions. Figure 5 shows a steady state of such an alloy. In steady state these regions did migrate with time, but they did not coarsen (at least coarsening was not observable for times of a factor of 10 longer than the time required to achieve the steady state). The precise boundaries of this two-phase region were difficult to determine precisely, but they extend approximately between values of ν for which the curves of L_{B32} and L_{umx} were 0.5. With increasing f, this two-phase region grew wider, primarily at the expense of the unmixed state. The domains in Fig. 5 are better described as $B32$ regions and unmixed regions with internal disorder, rather than fluctuations within a disordered alloy. The size of the ordered domains in steady state was found to decrease with increasing f. A fluctuation description is perhaps more appropriate for higher values of f.

IV. DISCUSSION

A. Thermodynamic partition function

Phase boundaries of thermodynamic phase diagrams are generally expected to change with temperature. To predict these changes analytically, we performed a low-temperature expansion of the partition function for the $B2$, $B32$, and unmixed alloys.[22] The idea behind this expansion is to identify the sensitivity of the free energy to small amounts of disorder, as might be expected at very low temperatures. For the $B2$ and unmixed alloys, the partition function, Z, was evaluated with the following terms:

$$Z=\exp\left[-\frac{N\varepsilon_0}{kT}\right]+N\exp\left[-\frac{N\varepsilon_0}{kT}\right]\exp\left[-\frac{\delta\varepsilon_1}{kT}\right]+4N\exp\left[-\frac{N\varepsilon_0}{kT}\right]\exp\left[-\frac{\delta\varepsilon_{2a}}{kT}\right]+3N\exp\left[-\frac{N\varepsilon_0}{kT}\right]\exp\left[-\frac{\delta\varepsilon_{2b}}{kT}\right]. \quad (6)$$

The first term is the Boltzmann factor for the perfect crystal, and the second term is the Boltzmann factor for the perfect crystal with one antisite atom. The third term accounts for one pair of antisite defects that are separated by a 1NN distance. The atoms in this pair have one fewer 1NN pair than two separated antisite defects. On the bcc lattice these dimer defects have a degeneracy of $4N$. The fourth term is for one pair of antisite defects separated by 2NN distances. Specific expressions for the energy differences $\{\delta\varepsilon\}$ are provided in Table I. First-neighbor pairs of antisite defects in the $B32$ structure required a slightly different treatment—the two antisite atoms could be located on sublattices of either like or unlike species.

Equation (6) was evaluated at the three phase boundaries: $B2/B32$ ($V_1>0$, $V_2=\frac{2}{3}V_1$), $B32$/umx ($V_1<0, V_2=-\frac{2}{3}V_1$), and $B32$/umx ($V_1=0$, $V_2<0$). The resulting free energy densities with respect to the disordered solid solution are

$B2/B32$ at ($V_{1AA}=V_{1BB}=V_1/2$, $V_{2AA}=V_2=\frac{2}{3}V_1$, $V_1>0$):

$$F_{B2}=-\frac{V_1}{2}-kT\left[\exp\left[-\frac{2V_1}{kT}\right]+4\exp\left[-\frac{3V_1}{kT}\right]+3\exp\left[\frac{-14V_1}{3kT}\right]\right], \quad (7)$$

$$F_{B32}=-\frac{V_1}{2}-kT\left[\exp\left[-\frac{2V_1}{kT}\right]+2\exp\left[-\frac{3V_1}{kT}\right]+2\exp\left[-\frac{5V_1}{kT}\right]+3\exp\left[-\frac{10V_1}{3kT}\right]\right], \quad (8)$$

$B32$/umx at ($V_{1AA}=V_{1BB}=V_1/2$, $V_{2AA}=V_2=-\frac{2}{3}V_1$, $V_1<0$):

$$F_{\text{umx}}=\frac{V_1}{2}-kT\left[\exp\left[\frac{2V_1}{kT}\right]+4\exp\left[\frac{3V_1}{kT}\right]+3\exp\left[\frac{14V_1}{3kT}\right]\right], \tag{9}$$

$$F_{B32}=\frac{V_1}{2}-kT\left[\exp\left[\frac{2V_1}{kT}\right]+2\exp\left[\frac{3V_1}{kT}\right]+2\exp\left[\frac{5V_1}{kT}\right]+3\exp\left[\frac{10V_1}{3kT}\right]\right], \tag{10}$$

$B2$/umx at ($V_1=0$, $V_{2AA}=V_{2BB}=V_2/2<0$):

$$F_{\text{umx}}=\frac{3V_2}{4}-kT\left[\exp\left[\frac{3V_2}{kT}\right]+4\exp\left[\frac{6V_2}{kT}\right]+3\exp\left[\frac{5V_2}{kT}\right]\right], \tag{11}$$

$$F_{B2}=\frac{3V_2}{4}-kT\left[\exp\left[\frac{3V_2}{kT}\right]+4\exp\left[\frac{6V_2}{kT}\right]+3\exp\left[\frac{5V_2}{kT}\right]\right]. \tag{12}$$

The presence of isolated antisite defects [the second term in Eq. (6)] causes no shifts of phase boundaries. It is therefore reasonable to neglect larger numbers of isolated antisite defects when writing the partition function of Eq. (6), at least for the purpose of finding shifts of phase boundaries. We note that Eqs. (7) and (8) were obtained previously.[23]

The low-temperature free energy expression of Eqs. (7)–(12) show that with increasing temperature, the $B32/B2$ and $B32$/umx phase boundaries shift by the same amounts. With increasing temperature, the $B2$ and unmixed phase regions encroach by the same amount into the $B32$ region. On the other hand, the $B2$/umx phase boundary is unchanged with temperature, at least to our level of approximation. We therefore expect that at moderately low temperatures, the $B2$/umx phase boundary will shift less with temperature than will the $B32/B2$ and $B32$/umx phase boundaries.

The shifts of phase boundaries caused by temperature predicted by the low-temperature expansion of the partition function were compared to results from the Monte Carlo simulations. The directions and magnitudes of the shifts were qualitatively consistent for the two methods, as we now discuss. However, the comparison of these shifts of phase boundaries required careful consideration of finite-size effects in the Monte Carlo simulations. In particular, the energy density of the unmixed state is affected strongly by the finite size of the lattice. While the ordered $B2$ and $B32$ phases become single domains in steady state, there must always be an interface between the regions of A atoms and B atoms in the unmixed state. The energy cost of this interface raises the internal energy density of the unmixed state with respect to the $B2$ and $B32$ states of order, causing these regions of ordered phase to encroach on the unmixed region of the phase diagram. To estimate this contribution to the internal energy, we prepared fully unmixed alloys on lattices of different sizes, with flat interfaces between the two species. We then determined the internal energy densities of these perfectly unmixed states. Using this excess energy density in a $T=0$ ground-state analysis of the $B2$/unmixed phase boundary, we found shifts of the phase boundary from the ideal $1/\nu=0$ to $1/\nu=0.0079$ and $1/\nu=0.0333$ for lattices with 128 and 32 unit cells on their edges, respectively. (Notice that these changes in $1/\nu$ scale satisfactorily with the surface/volume ratio of the lattices, as expected.) For comparison, the $B2$/umx phase boundary determined by steady states of Monte Carlo simulations was at $1/\nu=0.0322$ for lattices with 32 unit cells on their edges. Although the thermodynamic calculations of Sec. IV A predict no shift of the $B2$/umx phase boundary, the observed shift is explained adequately by the interface excess energy density of the unmixed state. The same finite-size effect on the energy of the unmixed alloy affects the shift of the $B32$/umx phase boundary. In this case there are competing thermodynamic and finite-size effects that provide opposing shifts of the position of the $B32$/umx boundary. Evidently, the finite-size effect of the surface excess energy density of the unmixed state is dominant, since the boundary shifts into the unmixed state with increasing temperature (and $f=0$). For a lattice with 32 unit cells on an edge, Monte Carlo results gave $\nu_c=-0.6632\pm0.0002$. This loss of surface excess energy when the alloy transforms from the unmixed state to the $B32$ state is qualitatively consistent with the large change in internal energy seen in Fig. 2(b) at $f=0.0003$. Finally, the $B32/B2$ phase boundary is not subject to any ambiguities from an internal interface. Monte Carlo simulations gave a $B32/B2$ phase boundary at $\nu_c=0.6728\pm0.0008$. This shift from the thermodynamic ground-state value of $\frac{2}{3}$ was due solely to the temperature effect, since in steady state both phases were single domains without antiphase domain

TABLE I. Terms of Eq. (6).

$\varepsilon_0^{B2}=-V_1+\frac{3}{4}V_2$	$\varepsilon_0^{B32}=-\frac{3}{4}V_2$	$\varepsilon_0^{\text{umx}}=V_1+\frac{3}{4}V_2$
$\delta\varepsilon_1^{B2}=4V_1-3V_2$	$\delta\varepsilon_1^{B32}=3V_2$	$\delta\varepsilon_1^{\text{umx}}=-4V_1-3V_2$
$\delta\varepsilon_{2a}^{B2}=7V_1-6V_2$	$\delta\varepsilon_{2ai}^{B32}=V_1+6V_2$; $\delta\varepsilon_{2aii}^{B32}=-V_1+6V_2$	$\delta\varepsilon_{2a}^{\text{umx}}=-7V_1-6V_2$
$\delta\varepsilon_{2b}^{B2}=8V_1-5V_2$	$\delta\varepsilon_{2b}^{B32}=5V_2$	$\delta\varepsilon_{2b}^{\text{umx}}=-8V_1-5V_2$

boundaries. Equations (7) and (8) provided the right sign for this shift, but the magnitude was low.

B. Phase boundaries with ballistic jumps

Figure 6 shows how ballistic jumps cause shifts of phase boundaries and the formation of two phase regions between the $B2$, $B32$, and unmixed states. The results of Fig. 6 were obtained from the data of Fig. 4, and analogous results for the $B2$/umx and the $B2/B32$[14] boundaries. The dashed lines in Fig. 6 are ν_c versus f. The values of ν_c were obtained by interpolation, and are believed to be fairly accurate. The solid curves in Fig. 6 are approximate boundaries of the two phase regions, defined as the values of ν for which the order parameters were about $\frac{1}{2}$. Although these boundaries of the two-phase regions are semiquantitative, they do show the right trend.

The shifts of the phase boundaries with the fraction of ballistic jumps (Fig. 6) are much larger than the shifts with temperature, T. The effects of temperature are almost negligible on the scale of Fig. 6, as can be seen by comparing the data points at $f=0$ to the ground-state values of ν_c (which were $+\frac{2}{3}, -\frac{2}{3}, \infty$). This smaller effect of temperature is still found when the shifts of the phase boundaries are normalized by the average defect density in one of the phases, for example, the $B32$ phase. We can monitor semiquantitatively the average defect density in the $B32$ phase in terms of $1-L$ (see Ref. 24). From Fig. 4, we see that for the thermodynamic case ($f=0$) around $\nu=0.7$, the value of $1-L$ for the $B32$ phase changes from 0 at $T=0$ to $1-L\approx 0.1$ at the nominal $T=1$ of the present simulations. From Fig. 4, we see that for a fraction of ballistic jumps of $f=0.05$, around $\nu=0.7$ there is a further change in $1-L$ from about 0.1 to about 0.2. Approximately, then, the fraction of ballistic jumps of 0.05 serve to create about as much disorder as does temperature itself. With temperature, the $B32$/umx phase boundary changes from $\nu=-\frac{2}{3}$ to $\nu=-0.663$, a change of ν_c of only 0.003. On the other hand, with a fraction of ballistic jumps of $f=0.05$, the change of ν_c is from $-\frac{2}{3}$ to -0.56, a much larger change of ν_c of 0.1. Although these numbers are imprecise, the shift of the phase boundary with ballistic jumps is much larger than expected if the change of ν_c were to scale with the defect concentration in the $B32$ phase in the same way as with temperature.

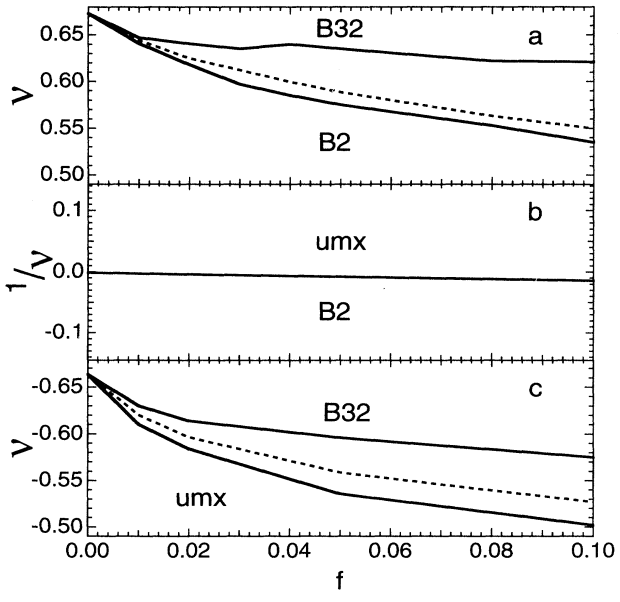

FIG. 6. The values of ν_c (dashed curve) and two-phase boundaries (solid curves) versus f for the pairs of phases: (a) $B32/B2$, (b) $B2$/umx, and (c) umx/$B32$. The $B2$/umx boundary was shifted downwards by the amount of $1/\nu=0.03$ to account for the finite-size effect in the Monte Carlo simulation.

Since the energy cost of an isolated antisite defect is about the same in both the $B32$ and unmixed alloys, we must understand the shift in phase boundary with f as originating with a type of high-energy defect structure in the unmixed alloy, or a larger number of defects in the unmixed alloy. Observation of selected planes of the two phases showed that in steady state the predominant defect was the antisite defect, and there tended to be more of them in the unmixed alloy than in the $B32$ alloys. The presence of the same fraction of ballistic jumps sustains a greater number of antisite defects in the unmixed alloy than in an alloy with $B32$ order. A greater number of antisite defects is also sustained in the $B2$ phase than in the $B32$ phase. The internal energies shown in Fig. 2 and 3 undergo a sharp change at the transition point. After accounting for finite-size effects of the Monte Carlo simulations, it is found that the changes in internal energy at both transitions, $B2\rightarrow B32$ and umx$\rightarrow B32$, were approximately the same.

The detailed mechanism responsible for these different effects of ballistic jumps on antisite defect populations remains unclear, but it must depend on details of the atom movements. We suggested earlier[14] that differences in the diffusional correlation factors for vacancy diffusion in the two phases could be responsible for thermal jumps that are less effective in eliminating the defects created by the ballistic jumps. With this reasoning, the diffusional correlation factors are larger (promoting atomic diffusion) in the $B32$ phase than in the unmixed or $B2$ states. Perhaps this is because the vacancy can migrate more freely along long channels of 1NN atoms of like type in the $B32$ structure, whereas the vacancy would tend to avoid one sublattice of the $B2$ structure, or would avoid some regions of the unmixed alloy.

It is tempting to compare the effects of ballistic atom movements to the effects of temperature, and assign an elevated effective temperature to an alloy in the presence of ballistic atom movements. This elevated effective temperature would be the temperature at which a similar alloy without ballistic atom movements would have the same equilibrium density of antisite (or other) defects. Unfortunately, the $B32\rightarrow B2$ transition that occurs with increased temperature does not occur with an increasing fraction of ballistic jumps; the opposite $B2\rightarrow B32$ transition occurs instead. While this could be explained by ballistic atom movements causing a larger increase in effective temperature for the $B2$ than the $B32$ phase, we

believe that using a different effective temperature for each phase causes the concept of effective temperature to lose much of its appeal. Another important limitation of the concept of an effective temperature arises because the relative populations of the different types of defects are generally expected to change with the fraction of ballistic jumps and with the particular phase. A single parameter of effective temperature is generally inadequate to account for the populations of all the different defect structures.

C. Phase diagrams

We expect that with small fractions of ballistic jumps, statistical fluctuations in their occurrence will cause spatial inhomogeneities in the defect densities. The internal energies of the unmixed state and $B2$ phase will be especially inhomogeneous, since the internal energies of these two phases are particularly sensitive to the presence of ballistic jumps. We believe that these inhomogeneities in internal energy density are responsible for the development of two-phase regions near the $B2/B32$ and $B32$/umx phase boundaries; locations with higher internal energy density will transform into the $B32$ phase. Two-phase microstructures of $B32$ phase plus $B2$ phase, or $B32$ phase plus unmixed state, were observed in Monte Carlo simulations when $f>0$. On the other hand, no two-phase microstructures of $B2$ phase plus unmixed state were observed in Monte Carlo simulations. This is as expected. Because both phases have similar stability with temperature and with f, local inhomogeneities in the internal energy density will not favor either the $B2$ phase or unmixed state. With larger f, the domain structures (such as those seen in Fig. 5) became smaller. This is as expected when fluctuations in the density of ballistic jumps occur over a smaller spatial scale. We do not have sufficient data to quantify this effect, however.

Figure 7(a) presents a ground-state phase diagram for bcc alloys with 1NN and 2NN interactions.[3,4] Figures 7(b) and 7(c) are schematic phase diagrams that include the presence of a finite temperature [Fig. 7(b)], and temperature plus ballistic jumps [Fig. 7(c)]. The effects of temperature on the boundaries between the $B2$, $B32$, and unmixed states are almost negligible on the scale of Fig. 7. A previous thermodynamic study of the $B32/B2$ phase boundary[23] seems consistent with our results.

The phase diagrams in Figs. 7(b) and 7(c) are our best efforts. Some of their features are more reliable than others. The $A2$ phase boundaries in Fig. 7(b) were obtained with only one point having mixed V_1 and V_2, but the straight lines between the axis intercepts are expected from mean-field calculations. The size and detailed shape of the $A2$ region in Fig. 7(c) are semiquantitative. Ballistic jumps cause an enlargement of the $A2$ region, drawn in Fig. 7(c) with estimates based on results from the two-dimensional square lattice.[15] A two-phase region might exist around the $A2$ phase, although it has not been reported for equiatomic alloys.[9-11] We performed a number of studies of alloys along the $B2/B32$ phase boundary at various values of V_1 from $+2$ to $+8$. These plots were similar to those of Fig. 4, and provided the values of ν_c and the $B2$ plus $B32$ two-phase boundaries in Fig. 7(c). The $B2$ phase plus unmixed state two-phase region in Fig. 7(c) is drawn in analogy to the $B32$ plus $B2$ two-phase region. For the two-phase region of the $B2$

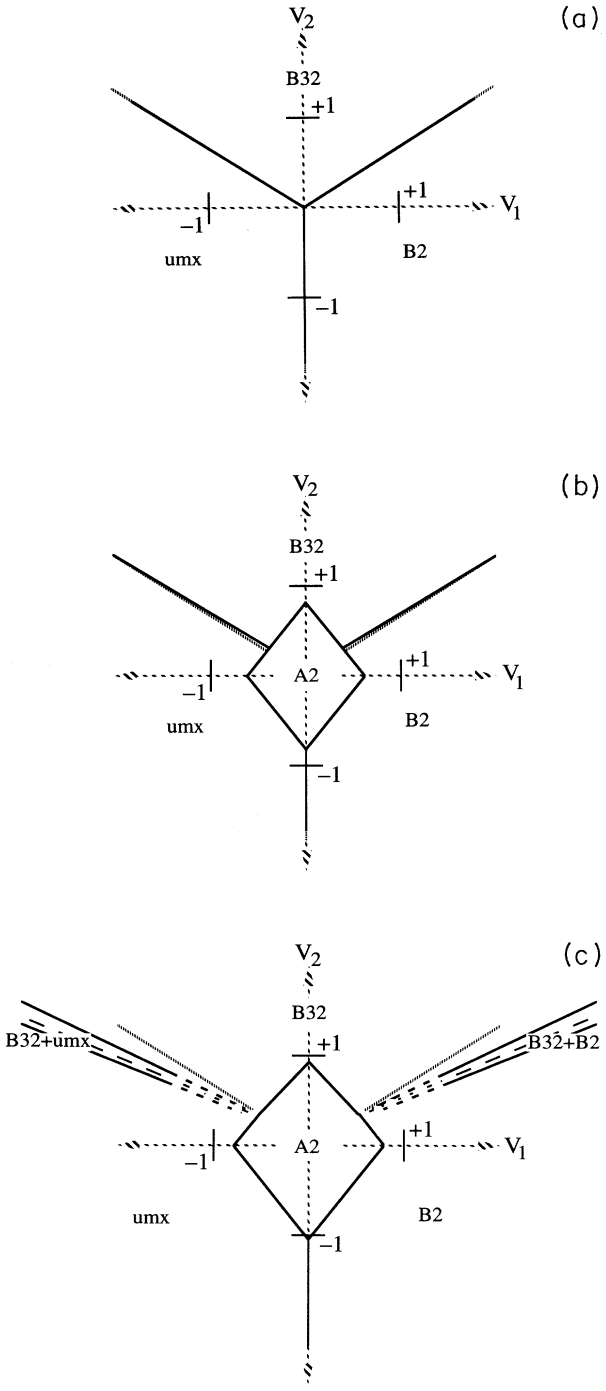

FIG. 7. Phase diagrams for the equiatomic bcc alloys: (a) thermodynamic ground state ($T=0, f=0$), (b) thermodynamic case at finite temperature ($T\approx 1, f=0$), (c) with ballistic jumps at finite temperature ($T\approx 1, f\approx 0.1$). Dotted lines have slopes $+\frac{2}{3}$ and $-\frac{2}{3}$.

phase plus unmixed state, we have data only for one magnitude of V_1 (the data of Fig. 4), but these data are similar to those for the $B32/B2$ two-phase region. Although we examined many alloys along the $B2$/umx boundary, we did not find any two-phase region of the $B2$ phase plus unmixed state. We therefore did not include a $B2$ phase plus unmixed state two-phase region in Fig. 7(c), although it might exist as a very narrow region.

V. CONCLUSION

We used Monte Carlo simulations to determine phase diagrams of equiatomic binary bcc alloys. Atom movements occurred by means of a vacancy mechanism with two types of atom movements: (1) thermal atom movements consistent with activated state rate theory, and (2) ballistic atom movements that were statistically random. Four phases exist on a bcc lattice with 1NN and 2NN interatomic potentials: $B32$ order, $B2$ order, an unmixed state of A- and B-rich regions, and a disordered $A2$ phase. The goal of our work was to measure and understand the shifts in the boundaries between the first three of these phases as a function of temperature and fraction of ballistic atom movements.

We found that in thermodynamic alloys, with increasing temperature the phase boundaries involving the $B32$ phase receded under the growth of the regions of the $B2$ phase and the unmixed state. A low-temperature expansion of the partition function showed that the higher energy for defect clusters in the $B32$ phase explained approximately the weak recession with temperature of the $B32$ phase boundaries. The opposite behavior was found in the presence of ballistic atom movements; there was a strong encroachment of the region of $B32$ phase into the regions of $B2$ and unmixed phases. The presence of ballistic atom movements therefore cannot be considered as a simple increase of temperature. In the presence of ballistic atom movements there are fewer defects in the $B32$ phase (which then has a lower internal energy) than in the $B2$ and unmixed states. While the detailed reason for this difference remains unclear, it is expected to depend on the kinetic mechanism. The phase boundary between the state of $B2$ order and the unmixed state shifted much less with temperature than did the boundaries involving the $B32$ phase. Another feature of the phase diagram in the presence of ballistic atom movements was the formation of two-phase regions between the $B32$ phase and the $B2$ phase, and between the $B32$ phase and the unmixed state. The width of these two-phase regions increased with increasing fraction of ballistic atom movements, and with decreasing temperature.

ACKNOWLEDGMENTS

We thank Dr. L. Anthony for stimulating discussions. This work was supported by the NSF under Contract No. DMR-9213447.

[1]E. Ising, Z. Phys. **31**, 253 (1925).
[2]L. Onsager, Phys. Rev. **65**, 117 (1944).
[3]M. J. Richards and J. W. Cahn, Acta Metall. **19**, 1263 (1971).
[4]S. M. Allen and J. W. Cahn, Acta Metall. **20**, 423 (1972).
[5]G. Martin, Phys. Rev. B **30**, 1424 (1984).
[6]P. Bellon and G. Martin, Phys. Rev. B **39**, 2403 (1989).
[7]E. Salomons, P. Bellon, F. Soisson, and G. Martin, Phys. Rev. B **45**, 4582 (1992).
[8]P. Bellon, Phys. Rev. B **45**, 7517 (1992).
[9]F. Soisson, P. Bellon, and G. Martin, Phys. Rev. B **46**, 11 332 (1992).
[10]P. Bellon, F. Soisson, and G. Martin, in *Diffusion in Ordered Alloys,* edited by B. Fultz, R. W. Cahn, and D. Gupta (TMS, Chicago, 1992).
[11]P. Bellon and G. Martin, Phys. Rev. B **38**, 2570 (1988).
[12]F. Haider, P. Bellon, and G. Martin, Phys. Rev. B **42**, 8274 (1990).
[13]W. Feller, *An Introduction to Probability Theory and Its Applications* (Wiley, New York, 1957), Vol. 1, Chap. 15.
[14]L. B. Hong, L. Anthony, and B. Fultz, J. Mater. Res. **10**, 126 (1995).
[15]L. B. Hong and B. Fultz, Phys. Rev. B **51**, 2687 (1995).
[16]K. C. Russell, Prog. Mater. Sci. **28**, 229 (1984).
[17]G. Martin and P. Bellon, in *Statistics and Dynamics of Alloy Phase Transformations,* edited by P. E. A. Turchi and A. Gonis (Plenum, New York, 1994).
[18]G. Nicolis and I. Prigogine, *Self-Organization in Nonequilibrium Systems* (Wiley, New York, 1977).
[19]L. Reinhard and P. E. A. Turchi, Phys. Rev. Lett. **72**, 120 (1994).
[20]L. Anthony and B. Fultz, J. Mater. Res. **4**, 1132 (1989); **9**, 348 (1994).
[21]L.-Q. Chen and A. G. Khachaturyan, Phys. Rev. B **44**, 4681 (1991); Scripta Metall. Mater. **25**, 61 (1991).
[22]F. Ducastelle, *Order and Phase Stability in Alloys* (North-Holland, Amsterdam, 1991), Sc. 5.1.2.
[23]M. Sluiter, P. Turchi, Z. Fu, and D. de Fontaine, Physica A **148**, 61 (1988).
[24]In the Bragg-Williams analysis, recall that $L \equiv (R-W)2/N$, where R is the number of correctly placed atoms on the sublattice of $N/2$ sites, and W is the number of wrongly placed ones. Therefore, $1-L=(R+W)2/N-(R-W)2/N=4W/N$. The concentration of antisite defects $c=(1-L)/2$.